CHEMISTRY OF MATERIALS

Article

pubs.acs.org/cm

Formation of Highly Ordered Alloy Nanoparticles Based on Precursor-Filled Latex Spheres

Achim Manzke,[†] Alfred Plettl,[†] Ulf Wiedwald,[†,*] Luyang Han,[†] Paul Ziemann,[†] Eyk Schreiber,[‡] Ulrich Ziener,[‡] Nicolas Vogel,[§] Clemens K. Weiss,[§] Katharina Landfester,[§] Kai Fauth,[∥] Johannes Biskupek,[⊥] and Ute Kaiser[⊥]

[†]Institute of Solid State Physics, Ulm University, Albert-Einstein-Allee 11, 89069 Ulm, Germany

[‡]Institute of Organic Chemistry III, Ulm University, Albert-Einstein-Allee 11, 89069 Ulm, Germany

[§]Max-Planck-Institute for Polymer Research, Ackermannweg 10, 55128 Mainz, Germany

[∥]Experimental Physics 4, Physical Institute, Würzburg University, Am Hubland, 97074 Würzburg, Germany

[⊥]Central Facility of Electron Microscopy, Ulm University, Albert-Einstein-Allee 11, 89069 Ulm, Germany

Supporting Information

ABSTRACT: An experimental approach is presented, allowing the preparation of substrate supported, hexagonally arranged metallic alloy nanoparticles with narrow size distributions, well-defined interparticle distances, and controlled chemical composition. The method is based on miniemulsion polymerization and isotropic plasma etching. Polystyrene (PS) and poly(methyl methacrylate) (PMMA) colloids—in the present study containing Fe- and Pt-precursor complexes in a predefined ratio—are deposited onto hydrophilic Si/SiO_2 substrates by dip-coating, forming a highly ordered monolayer. Contrary to colloidal lithography, here, precursor-filled polystyrene colloids serve as carriers for the alloy forming elements. After reactive ion etching and annealing, hexagonally ordered arrays of crystalline FePt nanoparticles are formed exhibiting the desired 1:1 Fe−Pt ratio, as revealed by detailed analysis after each preparation step. Formation of stoichiometric binary alloy FePt nanoparticles is confirmed by determining magnetic hysteresis loops, as well as applying aberration-corrected high-resolution transmission electron microscopy.

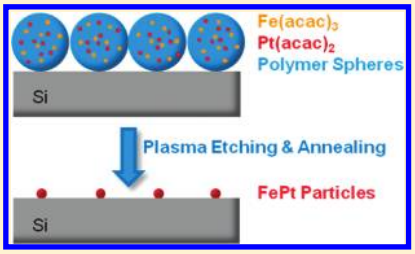

KEYWORDS: *miniemulsion, colloid monolayer, FePt, nanoparticles, colloidal lithography*

1. INTRODUCTION

Because of their size-dependent deviations from the corresponding bulk behavior, nanostructures open the perspective for novel functional devices.[1−5] Thus, much effort has been invested in the development of effective bottom-up preparation techniques. In the case of nanoparticles (NPs), such fabrication processes become even more demanding if additional requirements are imposed such as the preparation of ordered arrays of NPs, narrow size distributions and a well-defined chemical composition. While self-assembled latex spheres have been applied as templates and masks for subsequent deposition processes for many years to prepare highly ordered arrays of nearly triangular shaped structures with periods from micrometers down to 50 nm,[6,7] only recently more versatile direct methods were reported based on precursor loaded polystyrene[8] (PS) or polyacrylamide[9] colloids. Once these carriers are transferred onto a substrate forming a hexagonally ordered single layer, subsequent isotropic reactive ion etching (RIE) and annealing can transform the loaded colloids into metallic NPs at the original colloidal position. This approach has been successfully used to prepare highly ordered arrays of elemental Pt NPs.[8,10] For binary alloys, however, this loaded colloid process has not yet been developed, and it is the aim of the present work to demonstrate its successful application in that case as well.

For this purpose, FePt NPs were chosen, which offer attractive magnetic properties if prepared in the chemically ordered $L1_0$ phase. Especially, NPs of this type are top ranked candidates for magnetic data storage applications,[11,12] meeting the requirement of an as-high-as-possible magnetocrystalline anisotropy energy density (MAE) in order to overcome superparamagnetism at ambient temperature and save the information for a long period of time (typically for 10 years). For this application, however, two-dimensional ordered arrays appear necessary for facilitating the readdressing of previously encoded magnetic bits. Furthermore, narrow size distributions of the FePt NPs are mandatory to guarantee a small spread of the related hysteretic behavior.

Due to the attractive magnetic properties of FePt, realization of the above requirements has been attempted previously, and successful preparation of corresponding NPs was demonstrated based on colloidal[13,14] and micellar[15] approaches, as well as on physical gas phase condensation.[16,17] Although the achieved

Received: October 28, 2011
Revised: January 16, 2012
Published: January 17, 2012

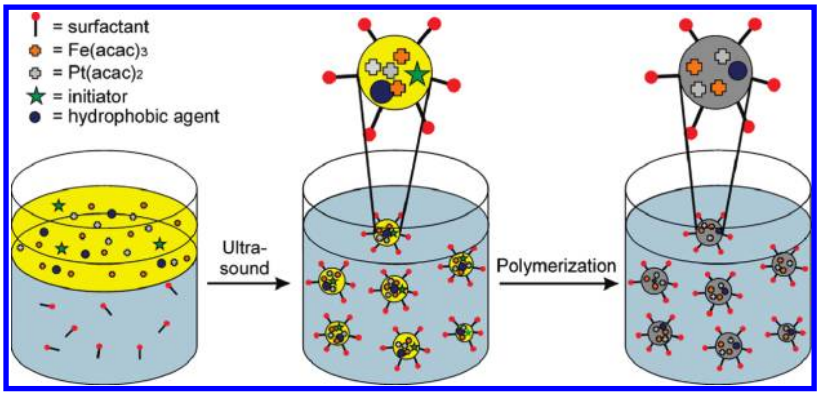

Figure 1. Schematics of the miniemulsion process applied for the fabrication of metal-complex loaded latex particles. Hexadecane (hydrophobic agent), V59 (initiator), and varying stoichiometric amounts of $Pt(acac)_2$ and $Fe(acac)_3$ were dissolved in styrene or methyl methacrylate (yellow) under continuous stirring. To this phase, a mixture of water (light blue) and SDS (surfactant) was added. Miniemulsions were achieved by ultrasound. Finally, the mixture was polymerized under continuous stirring.

magnetic properties significantly scatter in the literature, it is generally accepted that two crystallographic phases determine the magnetism of FePt alloys: (i) the cubic A1 phase leading to low MAE values and (ii) the tetragonal distorted, chemically ordered $L1_0$ phase exhibiting the attractive high MAE values.[18] Experimentally, however, it is mostly observed that FePt nanoparticles, as well as thin films, nucleate in the A1 phase,[19] since the transition into the thermodynamically favorable $L1_0$ phase is kinetically blocked. Still, by subsequent annealing, chemical order can be established to some degree, which in turn leads to the sought higher magnetic anisotropy. Note that the magnetic hardness of FePt may also be altered by surface chemistry or cover layers.[12,20] To circumvent this effect, we restricted our investigations to naked FePt particles on Si substrates.

Because the present work aims at a proof of principle that fabrication of binary alloy NPs is possible via precursor loaded colloids, RIE, and annealing, the choice of the FePt system is particularly suitable because alloy formation in magnetic nanoparticles can be proven not only by structural investigations but also by means of magnetism when the magnetic properties are examined before and after an annealing step. As will be demonstrated, it is exactly this annealing step that makes the present preparation route superior to the above-mentioned previous approaches. For the previous colloidal routes necessarily leading to small interparticle distances, annealing results in a significant tendency toward particle aggregation.[21] The above-mentioned micellar method, on the other hand, exploited its flexibility to increase the interparticle distance in order to avoid such annealing induced aggregation. The price to be paid, however, is a somewhat reduced degree of lateral order. At exactly this point, the idea of monodisperse latex particles sets in, which are loaded with metal precursors by applying the miniemulsion technique. Though, in the present article, feasibility of alloy formation via miniemulsions is exclusively proven with FePt NPs, this route offers much broader applicability to fabricate hexagonal patterns of alloy particles with control over their size and mutual distance.

2. PREPARATION OF MINIEMULSIONS

PS and poly(methyl methacrylate) (PMMA) colloids loaded with the hydrophobic metal complexes iron(III)acetylacetonate and platinum(II)acetylacetonate are prepared by miniemulsion polymerization.[22] This is the method of choice for the encapsulation of functional molecules into latex particles, as a stable emulsion is formed by sonication prior to polymerization, in which diffusion is effectively suppressed by the addition of an osmotic pressure agent (costabilizer) to the dispersed phase.[23−25] The corresponding interplay has been addressed as a nanoreactor-concept because each emulsion droplet acts as an individual entity during polymerization.[26,27] Thus, all functional molecules initially added to the monomer phase are statistically distributed among the individual nanodroplets. After polymerization, the composition of the latex particles closely resembles the composition of the monomer phase. For the encapsulation of two different metal complexes in a fixed/desired ratio, it is of crucial importance to have individual nanoreactors during the polymerization in order to retain the correct stoichiometry in the latex particles. This is a key difference of emulsion polymerization, where diffusion of monomers to the polymerization loci takes place.[28,29] As functional molecules added to the monomer will feature different diffusion coefficients, a stoichiometric encapsulation is impeded in that case.

Figure 1 sketches the miniemulsion process applied for the preparation of FePt NPs. Surfactant molecules (the ionic SDS (sodium dodecyl sulfate) or the nonionic Lutensol AT50) are added to the water phase while the monomer phase contains the initiator, the costabilizer (ultrahydrophobic component), and the hydrophobic metal complexes iron(III)acetylacetonate and platinum(II)acetylacetonate. The size of the final latex particles can be controlled by varying the amount of surfactant added.[30] The two phase system is sonicated to create a stable miniemulsion. The two possible degradation mechanisms, coagulation and Ostwald ripening, are effectively suppressed.[26] Coagulation is prevented by the electrostatic or steric repulsion of the surfactant molecules. Ostwald ripening is counteracted by an osmotic pressure that arises from the presence of the ultra-hydrophobic component.[31] After polymerization, a stable dispersion of latex particles containing metal complexes is formed.

3. CHARACTERIZATION OF ENCAPSULATION EFFICIENCIES

Prior to the formation of alloy NPs by RIE and their structural and magnetic characterization, the relative Fe and Pt contents in the polymer spheres before and after dialysis are thoroughly investigated as function of metal precursor content and

dx.doi.org/10.1021/cm203241p | Chem. Mater. 2012, 24, 1048−1054

surfactant concentration by inductively coupled plasma−optical emission spectrometry (ICP-OES).[32] Details of the experiments are given in the Supporting Information. Here, we briefly summarize the observations for Fe- and Pt-precursor loaded PS and PMMA spheres.

The encapsulation efficiency of iron(III)acetylacetonate in PS and PMMA nanospheres is always found close to the initial precursor concentration, independent of the SDS concentration (Supplementary Figures 1 and 2 in the Supporting Information). Precursor loading is similar for platinum(II)-acetylacetonate, with the exception of PS colloids with lower SDS concentrations (0.5−2 wt %). Here, strongly reduced encapsulation efficiencies of the Pt complex are found at high precursor concentrations (2 and 3 wt %). In the case of PMMA colloids, this loss of Pt precursor is not observed. After extensive dialysis of the obtained miniemulsions, the Fe content stays constant while the Pt content in the colloids decreases about 15% for PS and PMMA colloids. The loss of Pt complex, however, can be compensated by increasing the initial amount. Knowing that the loss of platinum complex is systematically close to 15% in all PS miniemulsions, stoichiometric dispersions can be synthesized with a small excess of platinum(II)acetylacetonate, thus compensating the loss during dialysis. Supplementary Figure 3 in the Supporting Information gives an example of this concept for miniemulsion1 (ME1).

Because the ionic surfactant SDS contains sulfur and sodium, successive reactive ion etching aiming at the formation of metal particles from precursor loaded colloids produces inorganic residues incorporated into NPs. Thus, strong variations of, for example, the magnetic properties have to be expected. We circumvented this concern by exchange of SDS with the nonionic surfactant Lutensol AT50 (containing only hydrogen, carbon, and oxygen). To guarantee matching the equiatomic ratio of Fe and Pt, the precursor loaded PS colloids are investigated by ICP-OES and energy dispersive X-ray spectroscopy (EDX). EDX reveals mean values of the Fe−Pt ratio of 1.03 for ME2 and 1.02 for ME3, averaged over many different sample positions. These findings are in good agreement with the initially weighted samples.

As the EDX measurements are performed only slightly above the detection limit, the more sensitive ICP-OES is additionally employed for determination of Fe−Pt ratios. For ME2 and ME3 we obtain an average Fe−Pt atomic ratio of 1.04 and 1.00, respectively. Hence, the initial precursor ratios, as well as the EDX results, are confirmed by ICP-OES. In the following we focus on the self-assembly of precursor-filled PS spheres and the metal particle formation and characterization

4. SELF-ASSEMBLY AND PARTICLE FORMATION

After synthesis of miniemulsions ME2 and ME3, a monolayer of the Fe and Pt precursor loaded PS particles ($ø \approx 175$ nm) is deposited on a silicon substrate. For the deposition, dispersions are diluted with purified water to 0.25 wt % solid content. The substrates are dip-coated under controlled atmospheric conditions (21 °C, 7% relative humidity), retracting the substrate from the solution at a constant velocity of 3 μm/s. To optimize the self-organized hexagonal order of the deposited PS spheres, strongly hydrophilic surfaces are essential. For this purpose, silicon wafers are exposed to oxygen plasma leading to the growth of surface oxides with a thickness above 4 nm, guaranteeing contact angles for water close to zero.[33] As a result, large areas of the substrates (5×10 mm^2) are coated with an almost perfect monolayer of loaded PS particles. Optical microscopy in Figure 2a reveals homogeneous coating of the Si substrates over macroscopic

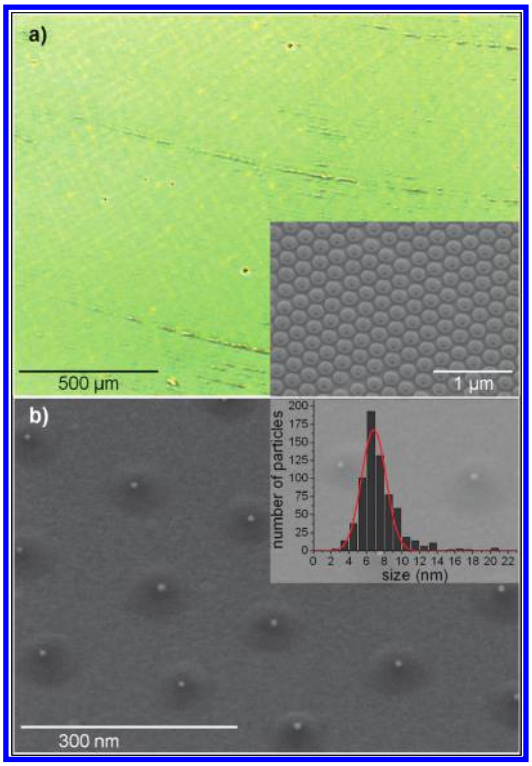

Figure 2. Monolayer of Fe- and Pt-precursor loaded PS spheres deposited by dip-coating onto hydrophilic Si/SiO_2 substrate over large scales, as demonstrated by optical microscopy (a). The inset of (a) presents a SEM image of PS particles at slightly reduced diameter by isotropic oxygen plasma treatment. A further homogeneous reduction of the diameter of the PS particles is achieved by longer plasma exposure times while their original hexagonal order is conserved. Subsequent annealing at 650 °C in vacuum for 120 min and at 1000 °C in oxygen atmosphere for 10 min leads to corresponding arrays of hexagonally ordered and single, oxidized FePt NP (b). The contrast deviations of the local particle surroundings compared to the rest of the surface is discussed below (cf. Figure 5 and text). The NPs exhibit a Gaussian size distribution with average size of 6.8 ± 1.4 nm (inset of b).

areas. Green areas consist of monolayers of 175 nm Fe- and Pt-precursor loaded PS spheres. Darker stripes are free of nanospheres. The typical area of perfectly ordered domains of PS spheres is about 25 μm^2.

The generation of arrays of FePt NPs by RIE processing basically follows an adopted route, initially established for elemental Pt NPs.[8,10,22] In a first step, hexagonally ordered PS arrays, as obtained by self-organization, are exposed to oxygen plasma, allowing a continuous and laterally homogeneous reduction of the particle diameters while keeping their positions fixed.[34] The scanning electron microscopy (SEM) image in the inset of Figure 2a demonstrates the success of the plasma etching: After 1 min in oxygen plasma, the size of the particles is homogeneously reduced while positions are maintained. Longer etching times result in smaller residual particles. Similar to the case of exclusively Pt-precursor filled PS particles, oxygen plasma treatment leads to a stationary diameter of about 25 nm after 25 min of etching. Supplementary Figure 4 in the Supporting Information presents a SEM image of this intermediate state. Here, the particles still consist of about 98

dx.doi.org/10.1021/cm203241p | Chem. Mater. 2012, 24, 1048−1054

vol % hydrocarbons, as compared to the final size of FePt NPs of about 7 nm. A subsequent annealing step at 650 °C, however, performed in a lamp furnace in vacuum for 120 min followed by 10 min at 1000 °C in oxygen atmosphere (partial pressure ≈1 mbar) removes the residual hydrocarbons and converts the many metal oxide nuclei into oxidized but single NPs, as demonstrated by the SEM image in Figure 2b. The size distribution of NPs (inset of Figure 2b) is determined from SEM BSE (backscattered electrons), as well as from TEM images. From Gaussian fitting (inset of Figure 2b), one finds an average diameter of 6.8 ± 1.4 nm (ME2). The distance between NPs is 175 nm and reflects the initial diameter of the PS spheres. Note that the NPs are at least partially oxidized for SEM and XPS investigations. The structure and magnetism of FePt alloy NPs presented below, however, have been determined in the metallic state after hydrogen plasma reduction and annealing (cf. Experimental Section).

5. STRUCTURE AND MAGNETISM OF ALLOY NANOPARTICLES

Next, these finally obtained NPs are analyzed with respect to their structure and composition including magnetic characterization. In this context it should be noted that such investigations are highly nontrivial due to the low particle density of typically 33 NPs per μm^2. A sufficiently sensitive method to provide information on the chemical composition of such small amounts of material is X-ray photoelectron spectroscopy (XPS). Figure 3 presents Fe-2p and Pt-4f spectra

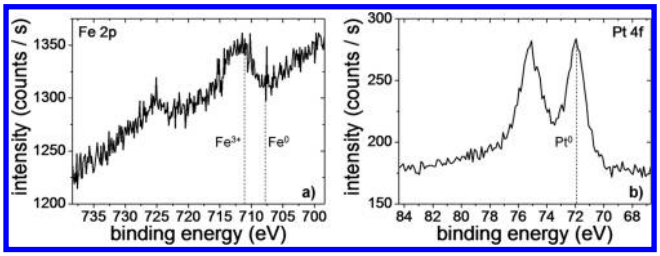

Figure 3. XPS spectra of FePt NPs on Si/SiO_2 (as shown in Figure 2b). The Fe-2p spectrum (a) predominantly shows Fe oxides, while the Pt-4f spectrum (b) is metallic. Composition analysis yields a Fe−Pt relative ratio of 1.02 (ME2).

of ME2 after etching and annealing steps described above. Comparison of energy positions and doublet separation to the literature (see the Experimental Section for details) clearly indicates that Fe oxides are formed while Pt remains in its Pt^0 state.[35,36] This observation is in line with studies on the oxidation behavior of FePt NPs prepared via reverse micelles.[37] From the intensity ratio of Fe-2p and Pt-4f core level spectra, the composition in the NPs is determined to be Fe−Pt = 1.02. This finding is consistent with the analysis of precursor filled PS spheres by EDX and ICP-OES. Thus, we can conclude that the etching process maintains the Fe−Pt ratio within the sample and nucleates the precursor material to partially oxidized particles. The results of the compositional analysis by EDX, ICP-OES, and XPS are summarized in Table 1. Within the uncertainties of the three techniques, it is obvious that the targeted equiatomic composition is conserved throughout all preparation steps.

For further structural and magnetic characterization of such FePt NPs, the representative ensemble ME2 is used (cf. Figure 2b). Initially, ME2 is reduced to the metallic state by H plasma

Table 1. Summary of the Fe−Pt Atomic Ratios as Determined by EDX, ICP-OES, and XPS[a]

sample	EDX	ICP	XPS
ME1		1.04	0.98
ME2	1.03	1.04	1.02
ME3	1.02	1.00	

[a]For the synthesis of miniemulsions, SDS (ME1) and Lutensol AT50 (ME2, ME3) were used as surfactants. Values given for ME1 are measured on the Si substrate supported FePt NPs fabricated from the dialyzed dispersion, whereas ME2 and ME3 have not been dialyzed. The desired value of 1 for the ratio is reached for all three ME and verified in good correlation by the three integral methods. The uncertainties of the experimental Fe−Pt ratio obtained by EDX is ±0.2 and for ICP-OES and XPS ±0.1. Therefore, the maximum deviation corresponds to a variation of stoichiometry of ±5% around the equiatomic ratio.

treatment at 300 °C for 20 min. Magnetism is probed by X-ray magnetic circular dichroism (XMCD) in the total electron yield mode. Figure 4a presents the raw X-ray absorption spectra at T = 12 K and H = ± 10 kOe switched at each photon energy. Note that the maximum dichroism observed in the total electron yield mode at the Fe-L_3 edge is as small as 0.42 pA measured on top of a background of 42 pA. In this extremely stable and sensitive setup, the magnetic characterization becomes feasible at a signal-to-noise ratio of about 30. A precise analysis of the Fe orbital and spin magnetic moment is, however, not possible under these conditions. Rather, the more robust ratio of the orbital-to-spin magnetic moment μ_L/μ_S = 0.07 ± 0.03 can be extracted from the XMCD spectrum (insert of Figure 4a). While the large relative error results from the limited signal-to-noise ratio, the μ_L/μ_S value is consistent with FePt alloys.[13,18,36] Element-specific magnetic hysteresis loops have been measured by scanning the sample current as a function of the external field of up to H = ± 30 kOe at the maximum dichroic signal (708 eV). In Figure 4b and c, hysteresis loops are shown at T = 12 K and T = 300 K after in situ reduction, that is, in the pure metallic state, and after annealing at T = 650 °C for 90 min in a hydrogen background of 1×10^{-4} mbar. After in situ reduction, FePt NPs exhibit a rather narrow hysteresis loop with a coercive field of 850 Oe and a superparamagnetic response at ambient temperature (not shown). Subsequent in situ annealing leads to partial chemical order accompanied by higher magnetic anisotropy.[38] Consequently, an enhanced coercive field of 1600 Oe is found at T = 12 K. Moreover, the shape of the hysteresis is significantly broadened with an irreversibility point at about 15 kOe. Most important for applications, we also observe an opening of the hysteresis at ambient temperature. The ferromagnetic portion is estimated to be about 30% at T = 300 K. Assuming Stoner−Wohlfarth particles, we find an effective anisotropy K_{eff} larger than 6.3×10^5 J/m^3.[39] This value only is about 10% of K_{eff} for perfectly $L1_0$ ordered FePt alloys, which we attribute to the limited annealing temperature and time, as well as Pt segregation effects.[15,18,19,37] From the XPS data obtained on the as-prepared NPs with Fe in an oxidized and Pt in its metallic state as given above, one might suspect that, after hydrogen plasma reduction, inhomogeneous NPs will result with a significant fraction of segregated pure Fe. Such an expectation can be excluded here, because pure Fe NPs would exhibit a much lower coercive field (typical value below 100 Oe). Thus, already at this point, we conclude that, after in situ reduction, indeed metallic FePt alloy NPs have been generated,

dx.doi.org/10.1021/cm203241p | Chem. Mater. 2012, 24, 1048−1054

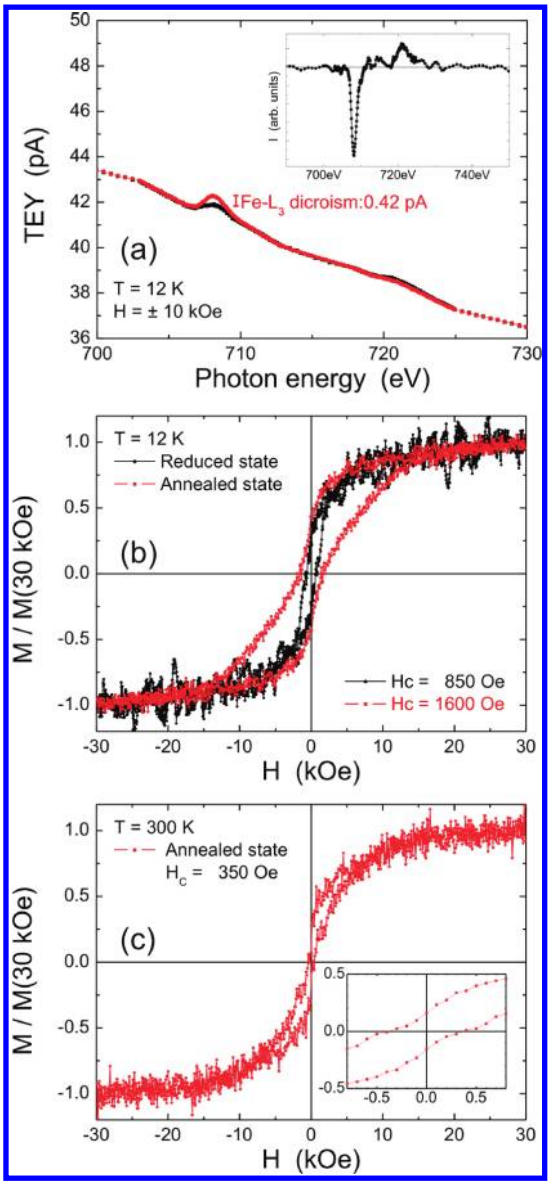

Figure 4. Magnetic characterization by XMCD of ME2. (a) Total electron yield currents at the Fe-$L_{3,2}$ edges in external fields of ±10 kOe using circularly polarized X-rays. The XMCD signal after normalization is shown in the insert. (b and c) Maximum dichroic signal at 708 eV used to measure the hysteresis loops before and after annealing (650 °C for 90 min) at 12 and 300 K. The insert in (c) is a magnification at low fields after 5-point averaging. Identical units apply.

which can be partly transformed into the magnetically attractive $L1_0$ phase by an annealing step at 650 °C for 90 min. However, comparing the MAE results with previous data on FePt NPs, we summarize that the MAE values are within the lower range of results found for NPs prepared by reverse micelles under similar conditions.

To corroborate this conclusion, after XMCD characterization, sample ME2 is investigated by transmission electron microscopy (TEM). Figure 5a presents an overview image of two FePt NPs on Si substrate in cross section. The distance between particles is similar to the observations by SEM (Figure 2b). The noticeable lens-shaped elevation is caused by a Si oxide layer growing faster under and around the FePt NPs, as compared to the plain substrate. This effect is known for Pt

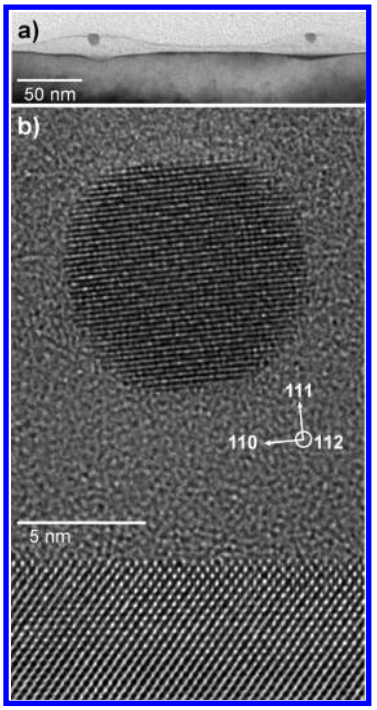

Figure 5. TEM image (top) showing two FePt NPs embedded in a lens-shaped silicon oxide layer on a silicon substrate. Silicon oxide is growing faster under and around the particles compared to naked substrate as a result of the catalytic effect of Pt. The HRTEM image clearly demonstrates the crystalline structure of the FePt NPs. By analysis of 13 NPs, an average lattice fringe spacing of (0.2225 ± 0.0058) nm is determined, as expected for (111) lattice planes of fcc FePt.

films on Si and is attributed to the catalytic activity of Pt for oxygen molecule dissociation, an important intermediate step for the oxidation process of Si.[40,41] Note that on other supports such as Al_2O_3 or MgO, such an effect does not exist. The high-resolution (HR)TEM image in Figure 5b clearly reveals the crystalline structure of this 9.5 nm FePt NP, which is slightly faceted along [111], [110], and [113] directions. The statistical evaluation of lattice constants by HRTEM is limited as a result of the large interparticle spacing. However, analysis of lattice fringe spacing of 13 nanocrystals by Fourier analysis using the crystalline Si substrate as reference delivers a value of (0.2225 ± 0.0058) nm in the [111] direction.[42,43] This value is larger than the (111) planar spacing of $Fe_{50}Pt_{50}$ bulk alloys (0.220 nm),[44] but it is smaller than that in pure Pt (0.226 nm), thus apparently pointing to a Pt-enriched FePt alloy. Care must be taken when translating the measured lattice spacing to the well-known linear dependence of the lattice constant with composition (Vegard's law[45]) in the bulk. A layerwise increase of the lattice parameter of up to 9% toward the surface has been observed in FePt icosahedra.[46] The reason for such local variations within single NPs has been attributed to Pt surface segregation.[37,47] We evaluated this effect by applying geometrical phase analysis (GPA).[48] Normalizing the lattice parameter averaged over the whole particle to 100%, the spacing is found varying from 98.5% for particle core columns to 101.5% toward the surface. Expecting a bulk-like lattice constant in the particle center, the (111) planar spacing is found to be 0.2192 nm, corresponding to a $Fe_{48}Pt_{52}$ alloy, in good agreement with compositions obtained by EDX, ICP, and XPS. Thus, the HRTEM results convincingly confirm FePt

dx.doi.org/10.1021/cm203241p | *Chem. Mater.* 2012, 24, 1048–1054

alloy formation in NPs prepared via precursor loaded PS spheres.

6. CONCLUSION

We have demonstrated that pure metal alloy NPs can be prepared via miniemulsions. In the present case, miniemulsion polymerization delivered Fe and Pt precursor loaded PS colloids in water, which then after dip-coating onto a substrate and exposure to various plasma and annealing steps finally form FePt alloy NPs. Detailed investigations of precursor ratio after each preparation step revealed a predictable composition of final NPs. Loaded PS colloids (175 nm) are self-organizing on Si substrates, forming hexagonal arrays, whereas the degree of order is conserved through all subsequent preparation steps. Finally, we deliver highly ordered arrangements of crystalline and chemically pure FePt NPs, as revealed by XPS, HRTEM, and magnetic measurements. Although not explicitly shown in the present work, the size and separation of such NPs can be controlled by the amount of metal-complexes incorporated and the initial diameter of PS colloids. The proof of principle of alloy NP formation on the route described in this article is by no means restricted to Fe and Pt complexes and can easily be expanded to other materials. However, miniemulsion and RIE processing have to be adjusted for new systems, and above all, a critical survey of the stoichiometry of alloys is indispensable.

7. EXPERIMENTAL SECTION

A. Materials. Styrene, hexadecane, and sodium dodecyl sulfate were purchased from Sigma Aldrich. To remove the inhibitor, styrene was distilled under reduced pressure prior to its use. The polymerization initiator 2,2′-azobis(2-methylbutyronitrile) (V59, Wako Chemicals) was used without further purification. Platinum(II)acetylacetonate and iron(III)acetylacetonate were purchased from Strem Chemicals.

B. Particle Synthesis. Miniemulsion polymerization was applied to synthesize the metal-complex containing latex particles.[27,28] Hexadecane (250 mg), 2,2′-azobis(2-methylbutyronitrile) (V59; 100 mg) and varying stoichiometric amounts of platinum(II)-acetylacetonate and iron(III)acetylacetonate were dissolved in 6 g of styrene under continuous stirring. To this phase, a mixture of water (24 g, Milli-Q quality) and SDS (30−300 mg) was added. After stirring for one hour at 1800 rpm and room temperature, miniemulsification was achieved by ultrasonicating the mixture under ice-cooling for 120 s with a 1/2" tip at 90% amplitude following a 10 s-pulse−10 s-break protocol, (Branson digital sonifier 450-D, Dietzenbach, Germany). Afterward, the mixture was heated to 72 °C and polymerized for 12 h under gentle continuous stirring. The dispersion was filtered using standard laboratory filters, and some were dialyzed (Visking dialysis tubes, MWCO = 14.000, Carl Roth GmbH). For the synthesis of ME2/ME3 styrene (2 g), hexadecane (90/80 mg), V59 (40/30 mg), platinum(II)acetylacetonate (20/21.5 mg), iron(III)acetylacetonate (30.8/33 mg), Lutensol AT50 (100 mg), and water (12/8 g) were used.

C. Deposition of PS Colloids. Prior to the deposition of Fe- and Pt-precursor loaded PS spheres, the dispersions were diluted with purified water to 0.25 wt %. Standard silicon substrates (CrysTec) were cut, cleaned with acetone and isopropanol in an ultrasonic bath, and exposed to oxygen plasma arriving at a strongly hydrophilic surface, for Si oxide layers of above 4 nm. Monolayers of loaded PS colloids were deposited on substrates by dip-coating at 3 μm s^{-1} under controlled atmosphere (21 °C, 7% relative humidity).

D. Etching of PS Colloids. Monolayer films of precursor-loaded PS particles were exposed to isotropic oxygen plasma (0.1 mbar, 100 W, −11 V dc-Bias, 300 K) delivered by a commercial etching machine (Oxford Plasmalab 80 Plus RIE). The annealing step was undertaken in a commercial rapid thermal annealing furnace (RTP-1200-100, UniTemp). Samples were annealed at 650 °C for 120 min in high vacuum and subsequently at 1000 °C for 10 min in 1 mbar oxygen atmosphere.

E. SEM Characterization. Samples were analyzed by SEM (Hitachi S-5200) directly after dip-coating, etching, and annealing steps without any further sample treatment. For EDX (EDAX Ametek) special samples were prepared on Si substrates. Miniemulsions ME2 and ME3 were dried and dissolved in THF dissolving precursor-loaded PS particles. This solution (15 μL) was dried on Si substrates in ambient conditions. The resulting continuous layer was strongly charging. For reasonable imaging quality, a 10 nm amorphous carbon film was evaporated on top. The compositions of ME2 and ME3 were determined from 16 and 8 measurements, respectively, at different sample positions using an acceleration voltage of 30 kV, 1 μA emission current, and 30 min acquisition time.

F. ICP-OES. Elemental analysis by inductively coupled plasma in the optical emission spectroscopy mode had a resolution of <1 ppm. Measurements on SDS containing nanospheres were performed with an ACTIVA M spectrometer (Horiba Jobin Yvon, Bernsheim, Germany) equipped with a Meinhardt-type nebulizer, a cyclone chamber at 1250 W forward plasma power, 12 L min^{-1} Ar flow and 15 rpm pump flow. The colloidal dispersions were diluted with water to 0.1 wt % of colloids and sonicated for 3 min prior to investigation. All samples and metal standard solutions contained 0.75 wt % sodium dodecyl sulfate following a previously established protocol.[37] The Ar emission line at 404.442 nm was used as reference. Measurements were performed using four different standard concentrations, at least two different elemental emission lines, and 5 s integration time. As baseline correction, a dynamic underground correction was used. Lutensol containing nanospheres (300 μL) were measured with a VARIAN-VISTA simultaneous spectrometer.

G. XPS Analysis. XPS was performed on partially oxidized samples prepared from ME1 and ME2 in an electron spectrometer (Phi-5800, Physical Electronics), equipped with a monochromatic X-ray source using Al Kα radiation (1486.6 eV) at an energy resolution of 0.6 eV. As a reference, pure Pt NPs were prepared on Si/SiO$_x$, similarly to the FePt NPs. Si-2p peak positions for both samples were used for calibration. These are almost identical and in good agreement with the reference value of 102.3 eV.[35] For both samples, the Pt-4f doublet separation is 3.3 eV that coincides with the metal reference data.[35] The Pt peak positions for the Pt NPs match the reference value of 71.3 eV, whereas the Pt-4f peaks for the FePt alloy NPs are shifted toward higher values (71.9 eV). This chemical shift is slightly larger than expected for equiatomic FePt alloys (0.2 eV) but much smaller than the expectation for PtO$_x$ (>74.2 eV). Fe-2p and Pt-4f peak areas have been evaluated for composition analyses using a Shirley background subtraction.[49]

H. Magnetic Measurements. Magnetic properties of ME2 were characterized by X-ray magnetic circular dichroism in the total electron yield mode in external fields of up to 30 kOe at beamline PM3 at BessyII synchrotron facility (Helmholtz-Zentrum Berlin). Prior to measurements, the sample was in situ reduced in H plasma at 300 °C for 20 min. Magnetic hysteresis loops were taken at the Fe-L$_3$ maximum dichroic signal before and after an additional in situ annealing step at 650 °C for 90 min.

I. TEM. For TEM investigations, the samples were cut into pieces (diamond wire saw), mechanically ground, dimpled, and polished to a thickness of <5 μm (Gatan dimple grinder). Low angle (10°) argon ion etching with energies of 5 to 1 keV (Fischione 1010 ion mill) was used to achieve electron transparency with lamella thicknesses smaller than 100 nm. TEM investigations were carried out using an aberration-corrected FEI Titan 80-300 microscope operating at 300 kV.

■ ASSOCIATED CONTENT

Ⓢ Supporting Information

Different encapsulation efficiencies of Fe(acac)$_3$ and Pt(acac)$_2$ in the miniemulsion process were determined for PS and PMMA spheres as function of SDS concentration. Excess of Pt(acac)$_2$ was used for fine-tuning the final FePt NP

composition at the equiatomic ratio. This information is available free of charge via the Internet at http://pubs.acs.org/.

AUTHOR INFORMATION

Corresponding Author

*E-Mail: ulf.wiedwald@uni-ulm.de.

Notes

The authors declare no competing financial interest.

ACKNOWLEDGMENTS

We thank Paul Walther (Ulm) for access to the SEM instrument and the training of students. We are grateful to Thomas Diemant (Ulm) for measuring the XPS spectra of FePt NPs. Beamline support by Thorsten Kachel and Helmut Pfau (Helmholtz Zentrum Berlin) at beamline PM-3 of BessyII synchrotron facility is kindly acknowledged. Finally, we acknowledge financial support by the Deutsche Forschungsgemeinschaft via SFB 569 and the Baden-Württemberg Stiftung via Kompetenznetz Funktionelle Nanostrukturen. N.V. acknowledges funding from the Materials Science in Mainz (MAINZ) graduate school.

REFERENCES

(1) Volokitin, Y.; Sinzig, J.; de Jongh, L. J.; Schmid, G.; Vargaftik, M. N.; Moiseeviet, I. I. *Nature* **1996**, *384*, 621−623.

(2) Zhang, H.; Gilbert, B.; Huang, F.; Banfield, J. F. *Nature* **2003**, *424*, 1025−1029.

(3) Brechignac, C.; Houdy, P.; Lahmani, M. *Nanomaterials and Nanochemistry*; Springer: Berlin, Germany, 2007.

(4) Boyen, H.-G.; Kästle, G.; Weigl, F.; Ziemann, P.; Schmid, G.; Garnier, M. G.; Oelhafen, P. *Phys. Rev. Lett.* **2001**, *87*, 276401.

(5) Boyen, H.-G.; Kästle, G.; Weigl, F.; Koslowski, B.; Dietrich, C.; Ziemann, P.; Spatz, J. P.; Riethmüller, S.; Hartmann, C.; Möller, M.; Schmid, G.; Garnier, M. G.; Oelhafen, P. *Science* **2002**, *297*, 1533−1536.

(6) Fischer, U. Ch.; Zingsheim, H. P. *J. Vac. Sci. Technol.* **1981**, *19*, 881−885.

(7) Kitaev, V.; Ozin, G. A. *Adv. Mater.* **2003**, *15*, 75−78.

(8) Manzke, A.; Pfahler, C.; Dubbers, O.; Plettl, A.; Ziemann, P.; Crespy, D.; Schreiber, E.; Ziener, U.; Landfester, K. *Adv. Mater.* **2007**, *19*, 1337−1341.

(9) Kobitskaya, E.; Ekinci, D.; Manzke, A.; Plettl, A.; Wiedwald, U.; Ziemann, P.; Biskupek, J.; Kaiser, U.; Ziener, U.; Landfester, K. *Macromolecules* **2010**, *43*, 3294−3305.

(10) Manzke, A.; Vogel, N.; Weiss, C. K.; Ziener, U.; Plettl, A.; Landfester, K.; Ziemann, P. *Nanoscale* **2011**, *3*, 2523−2528.

(11) Sun, S.; Murray, C. B.; Weller, D.; Folks, L.; Moser, A. *Science* **2000**, *287*, 1989−1992.

(12) Antoniak, C.; Gruner, M. E.; Spasova, M.; Trunova, A. V.; Römer, F. M.; Warland, A.; Krumme, B.; Fauth, K.; Sun, S.; Entel, P.; Farle, M.; Wende, H. *Nature Commun.* **2011**, *2*, 528.

(13) Antoniak, C.; Lindner, J.; Spasova, M.; Sudfeld, D.; Acet, M.; Farle, M.; Fauth, K.; Wiedwald, U.; Boyen, H.-G.; Ziemann, P.; Wilhelm, F.; Rogalev, A.; Sun, S. *Phys. Rev. Lett.* **2006**, *97*, 117201.

(14) Salgueiriño-Maceira, V.; Liz-Marzán, L. M.; Farle, M. *Langmuir* **2004**, *20*, 6946−6950.

(15) Ethirajan, A.; Wiedwald, U.; Boyen, H.-G.; Kern, B.; Han, L.; Klimmer, A.; Weigl, F.; Kästle, G.; Ziemann, P.; Fauth, K.; Schütz, G.; Jun, C.; Behm, R. J.; Büttner, M.; Romanyuk, A.; Oelhafen, P.; Walther, P.; Biskupek, J.; Kaiser, U. *Adv. Mater.* **2007**, *19*, 406−410.

(16) Rellinghaus, B.; Stappert, S.; Acet, M.; Wassermann, E. F. *J. Magn. Magn. Mater.* **2003**, *266*, 142−154.

(17) Dmitrieva, O.; Spasova, M.; Antoniak, C.; Acet, M.; Dumpich, G.; Kästner, J.; Farle, M.; Fauth, K.; Wiedwald, U.; Boyen, H.-G.; Ziemann, P. *Phys. Rev. B* **2007**, *76*, 064414.

(18) Wiedwald, U.; Han, L.; Biskupek, J.; Kaiser, U.; Ziemann, P. *Beilstein J. Nanotechnol.* **2010**, *1*, 24−47.

(19) Lyubina, J.; Rellinghaus, B.; Gutfleisch, O.; Albrecht, M. *Handb. Magn. Mater.* **2011**, *19*, 291−407.

(20) Serantes, D.; Spasova, M.; Baldomir, D.; Farle, M.; Salgueirino, V. *Chem. Mater.* **2010**, *22*, 4103−4110.

(21) Dai, Z. R.; Sun, S.; Wang, Z. L. *Nano Lett.* **2001**, *1*, 443−447.

(22) Schreiber, E.; Ziener, U.; Manzke, A.; Plettl, A.; Ziemann, P.; Landfester, K. *Chem. Mater.* **2009**, *21*, 1750−1760.

(23) Landfester, K. *Annu. Rev. Mater. Res.* **2006**, *36*, 231−279.

(24) Landfester, K. *Angew. Chem.-Int. Edit.* **2009**, *48*, 4488−4507.

(25) Landfester, K.; Weiss, C. K. *Adv. Polym. Sci.* **2010**, *229*, 1−49.

(26) Landfester, K.; Bechthold, N.; Förster, S.; Antonietti, M. *Macromol. Rapid Commun.* **1999**, *20*, 81−84.

(27) Landfester, K.; Bechthold, N.; Tiarks, F.; Antonietti, M. *Macromolecules* **1999**, *32*, 5222−5228.

(28) Harkins, W. D. *J. Am. Chem. Soc.* **1947**, *69*, 1428−1444.

(29) Hansen, F. K.; Ugelstad, J. *J. Polym. Sci., Part A−1: Polym. Chem.* **1978**, *16*, 1953−1979.

(30) Landfester, K. *Macromol. Rapid Commun.* **2001**, *22*, 896−936.

(31) Webster, A. J.; Cates, M. E. *Langmuir* **1998**, *14*, 2068−2079.

(32) Vogel, N.; Hauser, C. P.; Schuller, K.; Landfester, K.; Weiss, C. K. *Macromol. Chem. Phys.* **2010**, *211*, 1355−1368.

(33) Williams, R.; Goodman, A. M. *Appl. Phys. Lett.* **1974**, *25*, 531−532.

(34) Plettl, A.; Enderle, F.; Saitner, M.; Manzke, A.; Pfahler, C.; Wiedemann, S.; Ziemann, P. *Adv. Funct. Mater.* **2009**, *19*, 3279−3284.

(35) Wagner, C. D.; Naumkin, A. V.; Kraut-Vass, A.; Allison, J. W.; Powell, C. J.; Rumble, J., Jr. *NIST X-ray Photoelectron Spectroscopy Database*, Version 3.5. Available online: http://srdata.nist.gov/xps/; accessed, July 2011.

(36) Boyen, H.-G.; Kästle, G.; Weigl, F.; Ziemann, P.; Fauth, K.; Heßler, M.; Schütz, G.; Stahl, B.; Gajbhiye, N. S.; Ellrich, J.; Hahn, H.; Banhart, F.; Büttner, M.; Garnier, M. G.; Oelhafen, P. *Adv. Mater.* **2005**, *17*, 574−578.

(37) Han, L.; Wiedwald, U.; Kuerbanjiang, B.; Ziemann, P. *Nanotechnology* **2009**, *20*, 285706.

(38) Wiedwald, U.; Klimmer, A.; Kern, B.; Han, L.; Fauth, K.; Boyen, H.-G.; Ziemann, P. *Appl. Phys. Lett.* **2007**, *90*, 062508.

(39) Stoner, E. C.; Wohlfarth, P. *P. Philos. Trans. R. Soc. London* **1948**, *A240*, 599−642.

(40) Kobayashi, H.; Yuasa, T.; Nakato, Y.; Yoneda, K.; Todokoro, Y. *J. Appl. Phys.* **1996**, *80*, 4124−4128.

(41) Kobayashi, H.; Yuasa, T.; Yamanaka, K.; Yoneda, K.; Todokoro, Y. *J. Chem. Phys.* **1998**, *109*, 4997−5001.

(42) Biskupek, J.; Kaiser, U. *J. Electron Microsc.* **2004**, *53*, 601−610.

(43) Biskupek, J.; Jinschek, J. R.; Wiedwald, U.; Bendele, M.; Han, L.; Ziemann, P.; Kaiser, U. *Ultramicroscopy* **2010**, *110*, 820−825.

(44) Landolt, H.; Madelung, O. *Numerical Data and Functional Relationships in Science and Technology, New series Group IV/5e*; Springer: Berlin, Germany, 1995.

(45) Denton, A. R.; Ashcroft, N. W. *Phys. Rev. A* **1991**, *43*, 3161−3164.

(46) Wang, R. M.; Dmitrieva, O.; Farle, M.; Dumpich, G.; Ye, H. Q.; Poppa, H.; Kilaas, R.; Kisielowski, C. *Phys. Rev. Lett.* **2008**, *100*, 017205.

(47) Müller, M.; Albe, K. *Phys. Rev. B* **2005**, *72*, 094203.

(48) Hytch, M. J.; Putaux, J.-L.; Penisson, J.-M. *Nature* **2003**, *423*, 270−273.

(49) Shirley, D. A. *Phys. Rev. B* **1972**, *5*, 4709−4714.